Nanoscale Advances

ROYAL SOCIETY OF CHEMISTRY

PAPER

View Article Online
View Journal | View Issue

Cite this: *Nanoscale Adv.*, 2025, **7**, 7588

Rosmarinic acid attenuates doxorubicin-induced cardiotoxicity: bio-nanocarrier system development and an *in vitro* study using H9c2 rat cardiomyocytes

Afnan Al-Hunaiti, *[a] Tuqa Abu Thiab,[b] Malek Zihlif,[c] Amin M. S. Abdul Majid,[d] Amer Imraish,[b] Yazan Batarseh[e] and Mohammad Al Shhab[f]

Doxorubicin (DOX) is a potent chemotherapeutic agent widely used to treat various cancers, but its application is restricted by dose-limiting cardiotoxicity. This study investigates the cardioprotective effects of rosmarinic acid (RosA), a natural polyphenol with antioxidant and anti-inflammatory properties, in reducing DOX-induced cardiotoxicity while maintaining its anticancer efficacy. A novel nanoparticle delivery system was developed by conjugating RosA and DOX onto polyethylene glycol (PEG)–chitosan nanoparticles (Dox–RosA–PEG–CS), characterized by a zeta potential of +14.2 mV, a hydrodynamic size of 305 ± 5 nm, and an encapsulation efficiency of 82%. The results from H9C2 cardiac myocytes exposed to DOX and RosA demonstrated that RosA mitigated cardiotoxicity by reversing DOX-induced transcriptomic alterations, including downregulating apoptosis-related, cardiac remodeling, and inflammatory signaling genes. Additionally, RosA suppressed markers of inflammation, such as C–C motif chemokine ligands 2 (CCL2) and 11 (CCL11), and inhibited troponin T expression, a key indicator of myocardial damage. Anticancer studies on MDA-MB-231 breast cancer cells confirmed that RosA did not compromise DOX's therapeutic efficacy. These findings suggest that RosA, when delivered in a nanoparticle system, holds promise as a safe and effective adjunctive therapy for reducing DOX-induced cardiotoxicity, offering a novel strategy for enhancing the clinical utility of DOX in cancer treatment.

Received 14th June 2025
Accepted 22nd September 2025

DOI: 10.1039/d5na00585j

rsc.li/nanoscale-advances

Introduction

Doxorubicin (DOX) is a highly effective chemotherapeutic agent widely used in treating various cancers, including breast cancer. However, its clinical use is limited by dose-dependent cardiotoxicity, involving oxidative stress, inflammation, apoptosis, and cardiac remodeling, which can lead to irreversible cardiac dysfunction.[1–3] While the precise mechanisms remain unclear, reactive oxygen species (ROS), cell death, and inflammation are key contributors.[4,5] Thus, there is a pressing need for adjuvant cardioprotective agents that reduce these effects without diminishing DOX's anticancer efficacy.[6]

Rosmarinic acid (RosA), a natural polyphenol abundant in Lamiaceae family plants such as rosemary (*Rosmarinus officinalis*), perilla (*Perilla frutescens*), sage (*Salvia officinalis*), and lemon balm (*Melissa officinalis*), where it comprises up to 3–6% of dry weight in some species, can also be synthesized *via* the esterification of caffeic acid and 3,4-dihydroxyphenyllactic acid.[7] RosA exhibits cardioprotective and cytoprotective effects in preclinical models through antioxidant, anti-inflammatory, and anti-apoptotic mechanisms, making it a candidate for alleviating chemotherapy-induced cardiac damage.

Nanoformulations enhance drug delivery by improving penetration, protecting against enzymatic degradation, increasing absorption, boosting loading efficiency, and extending circulation time, thereby enhancing bioavailability and targeted accumulation.[8–10] They improve biodistribution, pharmacokinetics, solubility, and therapeutic index while enabling precise delivery, stability, and reduced degradation.[11–13]

A critical research gap involves targeted systems for co-delivering cardioprotectants with chemotherapeutics to

[a]Department of Chemistry, School of Science, The University of Jordan, Queen Rania Al-Abdullah Street, Amman 11942, Jordan. E-mail: a.alhunaiti@ju.edu.jo
[b]Department of Biological Sciences, School of Science, The University of Jordan, Amman, Jordan
[c]Department of Pharmacology, School of Medicine, The University of Jordan, Amman, Jordan
[d]College of Health & Medicine, Australian National University, Eman Research Ltd, 10-14 Wormald Street, Symonston, Canberra, Australia
[e]Department of Pharmacology and Biomedical Sciences, University of Petra, Amman, Jordan
[f]Department of Neurosurgery, Medical Center-University of Freiburg, Freiburg im Breisgau, Germany

minimize cardiotoxicity while preserving antitumor activity. Prior studies highlight the drawbacks of free DOX, such as non-specific distribution and cardiac accumulation, emphasizing the need for bionanocarriers. Chitosan-based nanoparticles offer biocompatibility, biodegradability, and hydrophilic drug encapsulation, with PEGylation improving stability and circulation.[14] PEGylated liposomes and micelles have shown reduced cardiotoxicity *via* controlled release and targeting.[15–17] Accordingly, PEGylated chitosan nanoparticles were chosen here for chitosan's mucoadhesive and biodegradable traits, facilitating controlled release and uptake, while PEGylation enhances solubility, reduces immunogenicity, and prolongs circulation—ideal for co-delivering DOX and RosA.[18] Although prior reports indicate RosA's potential in mitigating DOX cardiotoxicity, this study integrates RosA and DOX into a nanocarrier platform to elucidate mechanistic insights into its cardioprotective effects against DOX toxicity. By leveraging RosA's bioactivities with nanoparticle delivery, we aim to provide a safer strategy for DOX-based therapies.[19]

Herein, we investigate the potential of RosA to attenuate DOX-induced cardiotoxicity using an *in vitro* model of H9c2 cardiac myocytes. Using nanoparticle delivery systems, we aim to evaluate the protective effects of RosA in combination with DOX on the transcriptomic, cellular, and functional levels. The cardioprotective mechanisms of RosA were assessed through changes in gene expression associated with apoptosis, inflammation, and cardiac remodeling. Furthermore, we evaluated whether RosA impedes DOX's anticancer activity in MDA-MB-231 breast cancer cells to ensure clinical translation. By combining both RosA and Dox in a nanocarrier, this approach targets the cardiotoxic side effects of Dox without compromising its therapeutic potential, highlighting the role of RosA as a promising adjunct in chemotherapeutic regimens.

Methods

RosA used was commercially available (98% purity), chitosan (average molecular weight 20 kDa, degree of deacetylation >90%), and polyethylene glycol (2000 Da). All solvents were purchased from Sigma-Aldrich and used as received. IR spectra were recorded (KBr discs, 4000–300 cm^{-1}) using a PerkinElmer RX1 FTIR spectrometer. The size and zeta potential of different NPs were determined by DLS (Zetasizer 3000 HS, Malvern Instruments, Malvern, UK). The NP suspensions were filtered with a 0.45 m filter, and each batch was analyzed in triplicate.

Experimental

Preparation of NPs

In brief, 0.15 g of rosmarinic acid was dissolved in 15 ml deionized water; after stirring for 0.5 h at 45C, 0.35 g doxorubicin was added to the solution dropwise. 2 g PEG (1.0 mmol)–chitosan solution was added to the Ros–Dox mixture and stirred for 1 h. The resulting solution was then dialyzed against water for 2 days and lyophilized. Lastly, the chitosan solution in 1 : 5 molar ratio PEG : chitosan was slowly added to the PEG solution, and the resulting suspension was washed with CH_2Cl_2/methanol (volume ratio: 4 : 1) and centrifuged at 8500 rpm for 10 min. The supernatant was removed. The above process was repeated three times, and the precipitate was rinsed with deionized water and lyophilized to obtain the desired NPs.

Determination of the encapsulation efficiency (EE)

The encapsulation efficiency was measured based on the absorbance value of RosA and Dox free, and when capsulated at 608 nm and 425 nm, respectively. The capsulated NP solution (5 ml) was sonicated for 5 min (pulse on 2.0 s, off 2.0 s) to release the drug from NPs. A microplate spectrophotometer (UV-384

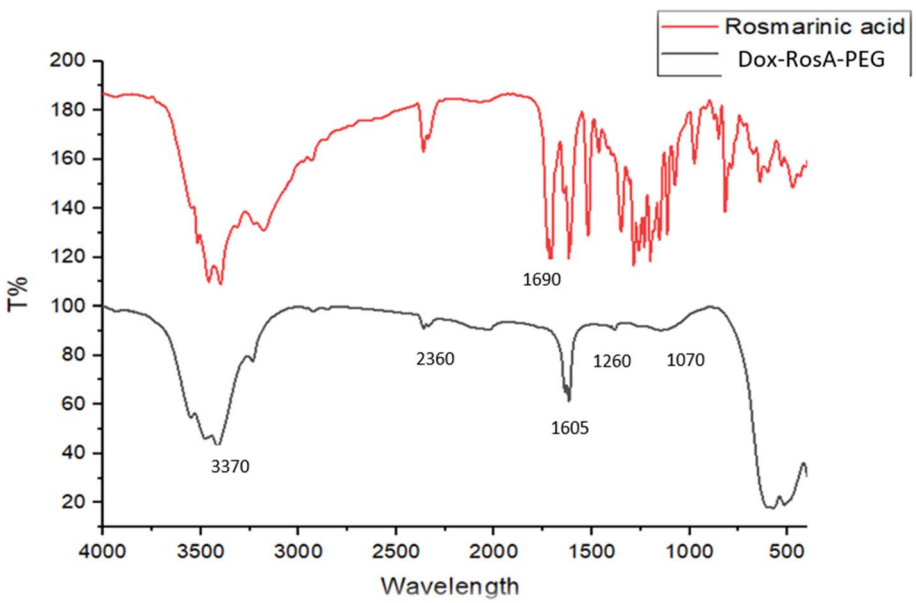

Fig. 1 The FTIR of rosmarinic acid and Dox–RosA–PEG prepared particles.

plus, Molecular Devices, Thermo Fisher Scientific Inc., Waltham, MA, USA) was used to calculate drug concentrations. The encapsulation efficiency (EE) was calculated as follows:

$$EE\% = (\text{the amount of total drug added} - \text{the amount of free drug in the supernatant})/(\text{the amount of totally added drug}) \times 100\%$$

Cell culture and maintenance

Rat cardiac myocytes-H9c2 (2-1) cells (CRL-1446™, ATCC) and MDA-MB-231 human breast cancer cell line (HTB-26™, ATCC) were allowed to proliferate in complete Dulbecco's Modified Eagle's Medium, supplemented with 10% fetal bovine serum (Corning, US), 1% penicillin streptomycin (Euroclone, Italy), 1% HEPES (Euroclone, Italy) buffer and 1% L-glutamine (Euroclone, Italy). Cells were incubated at 37 °C in a 5% CO_2 humidified atmosphere.

Evaluation of the cytotoxic effect of DOX–RosA–PEG NPs over cardiomyocytes and breast cancer cells

The amount of 7×10^3 of both cell types, H9c2 and MDA-MB-231 cells, were plated in a 96 well plate and left overnight to get attached. The day after, cells were treated with a serial dilution of Dox–RosA–PEG–CS NPs, where the concentrations started from 100 μg ml^{-1} down to 6 ng ml^{-1}. Control wells were kept running alongside the experiment and treated with media only. Treated cells were incubated for 72 h in a humidified atmosphere at 37 °C in a 5% CO_2 incubator. Then, cytotoxicity was measured using CellTiter 96® Non-Radioactive Cell Proliferation Assay – MTT (Promega), and the IC_{50} was calculated using GraphPad prism software.

Table 1 Size and ζ-potential of the prepared particle

NP type	Size (nm)	ζ-Potential
RosA coated by PEG (RosA–PEG)	228 ± 5	−18.3
Doxorubicin coated by PEG (Dox–PEG)	290 ± 5	−16.5
Doxorubicin–RosA coated (DOX–RosA–PEG)	305 ± 5	−14.2

Evaluation of the protective effect of DOX–RosA–PEG NPs over DOX treated cardiomyocytes

The amount of 100×10^3 of H9c2 cells were seeded per each well of 12 well plates and left overnight to firmly attach to the surface at 37 °C in a humidified 5% CO_2 incubator. The day after, the concentrations of 3.125 μg ml^{-1} of DOX-NPs and 6.251 μg ml^{-1} of DOX-NP-RoA-200 were applied over seeded H9c2 cells in triplicate. Control H9c2 wells were running beside and treated only with the same media used for treatment preparation. After 24 h treatment, RNA was harvested using RNeasy Mini Kit (Qiagen, USA), and the amount of 500 ng was reverse transcribed using PrimeScript™ 1st strand cDNA Synthesis Kit (Takara, Japan). Changes in the expression of genes responsible for cardiovascular diseases were investigated using the quantitative RT2 Profiler PCR array for Rat Cardiovascular Disease (PARN-174ZD, Qiagen). Data were analyzed using the online SABiosciences Qiagen company (Qiagen, USA) web page, where the delta cycle threshold ($\Delta\Delta C_t$) was used to calculate the fold change by which the genes were down-regulated or up-regulated.

Results

Characterization of the NPs

Fig. 1 compares the FTIR spectra of RosA, PEG–chitosan (PEG–CS), and the DOX–RosA–PEG–CS conjugate. The conjugate exhibits the expected broad O–H/N–H stretch at approximately 3370 cm^{-1} and a shift in the amide region from ~1630 cm^{-1} in

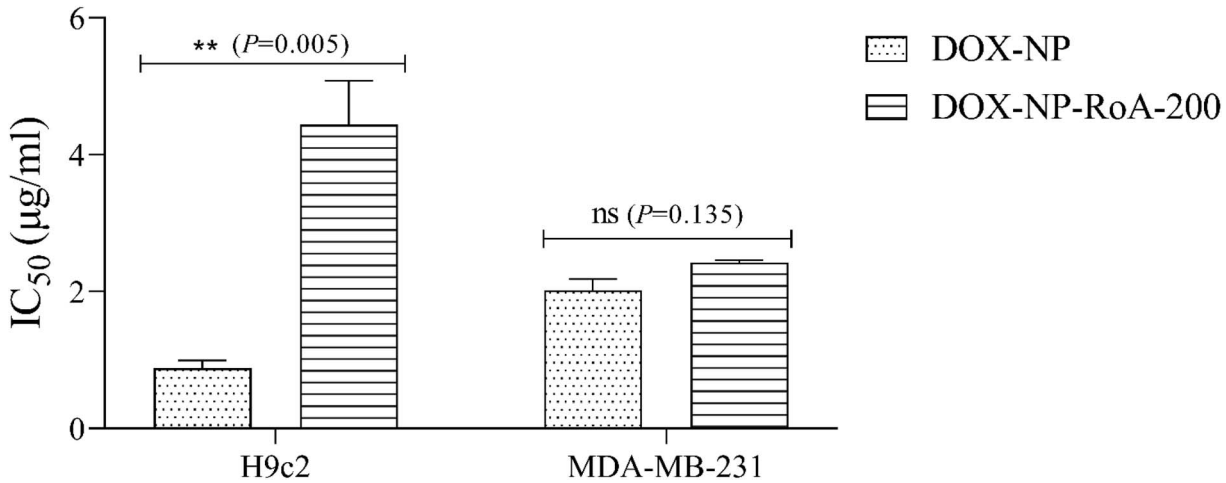

Fig. 2 IC_{50} of Dox-NP *vs.* DOX-NP-RoA-200 NPs against MDA-MB-231 and H9c2 cells. A serial dilution of both NP types was applied over both cell types for 72 h. MTT cytotoxicity assay was performed to measure the cytotoxic effect of NPs. The IC_{50} of DOX-NPs and DOX-NP-RoA-200 was calculated using the logarithmic trendline of cytotoxicity graphs (log(concentration *versus* inhibition)). Results are presented as the level of IC_{50} of both DOX-NPs and DOX-NP-RoA-200 treatment groups per each cell type. Further analysis using Student's *t*-test was performed to compare the cytotoxic effect of DOX-NPs and DOX-NP-RoA-200/cell type. ** Significance considered for $p < 0.01$.

Table 2 Gene annotation for upregulated and downregulated genes (cut-off point of 1.5 fold) for H9c2 cells exposed to DOX–PEG NPs

Gene symbol	Gene description	Fold change	Function
Maoa	Monoamine oxidase A	−1.79	Apoptosis
Nppa	Natriuretic peptide precursor A	−1.6	Apoptosis
Nppb	Natriuretic peptide precursor B	−3.07	Apoptosis
Snca	Synuclein, alpha (non A4 component of amyloid precursor)	−1.62	Apoptosis
Thbs2	Thrombospondin 2	−2.01	Apoptosis
Ubb	Ubiquitin B	−1.51	Apoptosis
Zyx	Zyxin	−1.71	Apoptosis
Col11a1	Cyclin-dependent kinase inhibitor 1B	−2.04	Cardiac remodeling
Col1a1	Collagen, type XI, alpha 1	−2.11	Cardiac remodeling
Col3a1	Collagen, type I, alpha 1	−2.65	Cardiac remodeling
Dcn	Decorin	−2.21	Cardiac remodeling
Dmd	Dystrophin	−2.86	Cardiac remodeling
F2r	Coagulation factor II (thrombin) receptor	−2.45	Cardiac remodeling
Fn1	Fibronectin 1	−1.95	Cardiac remodeling
Rtn4	Reticulon 4	−1.79	Cardiac remodeling
Ccnd1	Chemokine (C–C motif) ligand 2	−1.55	Cell cycle
Cdkn1b	Cyclin D1	−5.4	Cell cycle
Rarres1	Retinoic acid receptor responder (tazarotene induced) 1	−2.23	Cell cycle
Ctgf	Connective tissue growth factor	−3.98	Cell growth
Ptn	Pleiotrophin	−1.53	Cell growth
Spock1	Sparc/osteonectin, cwcv and kazal-like domains proteoglycan (testican) 1	−1.59	Cell growth
Actc1	Actin, alpha, cardiac muscle 1	−1.62	Sarcomere structural proteins
Myh10	Myosin, heavy chain 10, non-muscle	−3.12	Sarcomere structural proteins
Nebl	Nebulette	−1.62	Sarcomere structural proteins
Adra1b	Adrenergic, alpha-1B-, receptor	−2.44	Signal transduction
Agtr1a	Angiotensin II receptor, type 1a	−1.54	Signal transduction
Ar	Androgen receptor	−1.62	Signal transduction
Hmgcr	3-Hydroxy-3-methylglutaryl-coenzyme A reductase	−4.7	Signal transduction
Mapk1	Mitogen activated protein kinase 1	−2.08	Signal transduction
Mapk8	Mitogen-activated protein kinase 8	−1.82	Signal transduction
Npr3	Natriuretic peptide receptor C/guanylate cyclase C (atrionatriuretic peptidereceptor C)	−1.68	Signal transduction
Nr3c1	Nuclear receptor subfamily 3, group C, member 1	−1.91	Signal transduction
Nr3c2	Nuclear receptor subfamily 3, group C, member 2	−1.95	Signal transduction
Pde3b	Phosphodiesterase 3B, cGMP-inhibited	−2.46	Signal transduction
Pde7a	Phosphodiesterase 7A	−1.94	Signal transduction
Rassf1	Ras association (RalGDS/AF-6) domain family member 1	−3.63	Signal transduction
Cxcl12	Chemokine (C–X–C motif) ligand 12 (stromal cell-derived factor 1)	−4.48	Stress & immune response
S100a8	S100 calcium binding protein A8	−1.54	Stress & immune response
Creb5	Collagen, type III, alpha 1	−4.12	Transcriptional regulation
Enah	Enabled homolog (Drosophila)	−2.81	Transcriptional regulation
Hmgn2	High mobility group nucleosomal binding domain 2	−13.03	Transcriptional regulation
Msi2	Musashi RNA-binding protein 2	−3.49	Transcriptional regulation
Nfia	Nuclear factor I/A	−3.42	Transcriptional regulation
Nkx2-5	NK2 transcription factor related, locus 5 (Drosophila)	−1.67	Transcriptional regulation
Stat1	Signal transducer and activator of transcription 1	−2.18	Transcriptional regulation
Tcf4	Transcription factor 4	−2.29	Transcriptional regulation
Atp2a2	ATPase, Ca++ transporting, cardiac muscle, slow twitch 2	−1.62	Transporters
Atp5a1	ATP synthase, H+ transporting, mitochondrial F1 complex, alpha subunit 1	−1.55	Transporters
Aebp1	AE binding protein 1	1.85	Cardiac remodeling
Serpina3n	Serine (or cysteine) peptidase inhibitor, clade A, member 3N	2.31	Cardiac remodeling
Tnni3	Troponin I type 3 (cardiac)	1.51	Cardiac remodeling
Tnnt2	Troponin T type 2 (cardiac)	6.23	Cardiac remodeling
Sfrp4	Secreted frizzled-related protein 4	4.62	Cell growth
Crym	Crystallin, mu	5.35	Sarcomere structural proteins
Myh6	Myosin, heavy chain 6, cardiac muscle, alpha	3.46	Sarcomere structural proteins
Dusp6	Dual specificity phosphatase 6	1.55	Signal transduction
C6	Cardiac muscle	1.93	Stress & immune response
Ccl11	Complement component 6	2.8	Stress & immune response
Ccl2	Chemokine (C–C motif) ligand 11	1.56	Stress & immune response

PEG to ∼1605 cm^{-1}, consistent with conjugation-induced changes and overlap with aromatic bands. The carrier backbone is evident through strong C–O/C–O–C vibrations around 1070–1100 cm^{-1} (chitosan/PEG). RosA-specific features between 1700 and 1000 cm^{-1} are retained in the conjugate, including an ester C=O band at ∼1690 cm^{-1} (intensity increasing with RosA

Table 3 Gene annotation for upregulated and downregulated genes (cut-off point of 1.5 fold) for H9c2 cells exposed to Dox–RosA–PEG–CS NPs

Gene symbol	Gene description	Fold change	Function
Maoa	Monoamine oxidase A	−1.69	Apoptosis
Nppa	Natriuretic peptide precursor A	−6.6	Apoptosis
Nppb	Natriuretic peptide precursor B	−7.65	Apoptosis
Npr1	Natriuretic peptide receptor A/guanylate cyclase A (atrionatriuretic peptidereceptor A)	−1.52	Apoptosis
Pde3a	Phosphodiesterase 3A, cGMP inhibited	−1.52	Apoptosis
Snca	Synuclein, alpha (non A4 component of amyloid precursor)	−1.52	Apoptosis
Thbs2	Thrombospondin 2	−2.25	Apoptosis
Col11a1	Cyclin-dependent kinase inhibitor 1B	−1.53	Cardiac remodeling
Col3a1	Collagen, type I, alpha 1	−1.99	Cardiac remodeling
Dmd	Dystrophin	−2.26	Cardiac remodeling
F2r	Coagulation factor II (thrombin) receptor	−1.61	Cardiac remodeling
Rtn4	Reticulon 4	−1.79	Cardiac remodeling
Serpina3n	Serine (or cysteine) peptidase inhibitor, clade A, member 3N	−1.52	Cardiac remodeling
Tnni3	Troponin I type 3 (cardiac)	−2.54	Cardiac remodeling
Tnnt2	Troponin T type 2 (cardiac)	−1.79	Cardiac remodeling
Cdkn1b	Cyclin D1	−4.32	Cell cycle
G0s2	G0/G1switch 2	−1.23	Cell cycle
Rarres1	Retinoic acid receptor responder (tazarotene induced) 1	−3.71	Cell cycle
Ctgf	Connective tissue growth factor	−3.74	Cell growth
Ptn	Pleiotrophin	−5.29	Cell growth
Spock1	Sparc/osteonectin, cwcv and kazal-like domains proteoglycan (testican) 1	−1.59	Cell growth
Actc1	Actin, alpha, cardiac muscle 1	−1.52	Sarcomere structural proteins
Myh10	Myosin, heavy chain 10, non-muscle	−2.05	Sarcomere structural proteins
Myh6	Myosin, heavy chain 6, cardiac muscle, alpha	−1.52	Sarcomere structural proteins
Nebl	Nebulette	−1.52	Sarcomere structural proteins
Adra1a	Adrenergic, alpha-1A-, receptor	−1.52	Signal transduction
Adra1b	Adrenergic, alpha-1B-, receptor	−2.07	Signal transduction
Adra1d	Adrenergic, alpha-1D-, receptor	−1.54	Signal transduction
Adrb1	Adrenergic, beta-1-, receptor	−1.52	Signal transduction
Adrb2	Adrenergic, beta-2-, receptor, surface	−1.52	Signal transduction
Adrb3	Adrenergic, beta-3-, receptor	−1.52	Signal transduction
Agtr1a	Angiotensin II receptor, type 1a	−1.52	Signal transduction
Ar	Androgen receptor	−1.52	Signal transduction
Epor	Erythropoietin receptor	−1.69	Signal transduction
Frzb	Frizzled-related protein	−1.52	Signal transduction
Hmgcr	3-Hydroxy-3-methylglutaryl-coenzyme A reductase	−3.71	Signal transduction
Mapk1	Mitogen activated protein kinase 1	−1.53	Signal transduction
Pde3b	Phosphodiesterase 3B, cGMP-inhibited	−2.46	Signal transduction
Pde7a	Phosphodiesterase 7A	−1.94	Signal transduction
Rassf1	Ras association (RalGDS/AF-6) domain family member 1	−3.31	Signal transduction
Slc12a1	Solute carrier family 12 (sodium/potassium/chloride transporters), member 1	−1.52	Signal transduction
C6	Cardiac muscle	−1.65	Stress & immune response
Ccl11	Complement component 6	−1.52	Stress & immune response
Cxcl12	Chemokine (C–X–C motif) ligand 12 (stromal cell-derived factor 1)	−1.95	Stress & immune response
S100a8	S100 calcium binding protein A8	−1.52	Stress & immune response
Ccl2	Chemokine (C–C motif) ligand 11	−6.44	Stress & immune response
Creb5	Collagen, type III, alpha 1	−3.19	Transcriptional regulation
Enah	Enabled homolog (Drosophila)	−2.02	Transcriptional regulation
Hmgn2	High mobility group nucleosomal binding domain 2	−9.42	Transcriptional regulation
Nfia	Nuclear factor I/A	−2.62	Transcriptional regulation
Nkx2-5	NK2 transcription factor related, locus 5 (Drosophila)	−2.41	Transcriptional regulation
Tcf4	Transcription factor 4	−1.76	Transcriptional regulation
Sfrp4	Secreted frizzled-related protein 4	2.55	Cell growth

content), aromatic C=C bands near 1605 cm^{-1}, and a distinct band at ~1520 cm^{-1} attributable to RosA's aromatic ring that is absent in the carrier. Additionally, a band at ~1260 cm^{-1} (amide, C–N stretching/N/N–H bending) appears in the conjugate, consistent with the formation of a new amide linkage. Therefore, it can be said that successful coating with a nanocarrier is validated and supported by the characteristic PEG peaks.[18]

The particle size and the zeta potential of the prepared nanoparticles are represented in Table 1. The results can be discussed in terms of surface charge (zeta potential, in mV) and hydrodynamic size (in nm) of different nanoparticle

formulations: RosA–PEG with moderate negative charge and size (−18.3 mV; 228 ± 5 nm). The DOX-coated PEG nanoparticles also show a slightly negative charge, resembling RosA–PEGs. However, the charge is slightly less negative, likely due to the interaction of PEG with Dox, which may reduce the availability of negatively charged groups on the NP surface. Furthermore, the increase may also be due to the hydrophobic interaction between DOX and PEG chains and nanoparticle surfaces Dox–PEG (−16.5 mV; 290 ± 5 nm). Combining both DOX and RosA on the same PEGylated surface results in a significant shift in size and in charge toward a higher zeta potential for DOX–RosA–PEG (−14.2 mV; 305 ± 5 nm). The largest size results in greater structural complexity and, hence, an increase in hydrodynamic diameter. This size is still within the acceptable range for nanoparticle-based drug delivery, but is closer to the upper limit for optimal tumor penetration through the Enhanced Permeability and Retention (EPR) effect. Noteworthily, DOX is a cationic drug with an inherent positive charge, which likely dominates the surface charge of the nanoparticle when conjugated with RoA and PEG. The positive charge could enhance interactions with negatively charged cell membranes, improving cellular uptake, especially for cancer cells.

Encapsulation efficiency

As expected, the coating formed in a moderate size, with the most significant positive zeta potential but the highest drug loading capacity. The PEG : CS significantly impacted the loading capacity for DOX–RosA. This was because the assembly of DOX was directly correlated to the degree of PEG. Since DOX and RosA are hydrophobic molecules, the use of more significant amounts of DOX–RosA resulted in a higher encapsulation efficiency of 82%.

Cytotoxicity of DOX–RoA–PEG–CS NPs over cardiomyocytes and breast cancer cells

The synthesized NPs were purified and characterized by several analytical techniques and applied for anticancer efficacy against breast cancer cells (MDA-231) and cardiac H9c2 cells. Moreover, the toxicity of Dox coated with PEG (DOX–PEG) was also evaluated on the same set of cells to trace the protective effect of RosA against the cardiac toxicity of doxorubicin, a chemotherapy agent. As shown in Fig. 2, DOX–PEG alone showed potent toxicity on the tested cells, with measured IC_{50}s values 2 μM and 0.8 μM on MDA-231 and H9c2 cardiac cells, respectively. Combining doxorubicin with rosmarinic acid in one drug (DOX–RosA–PEG) was suggested to minimize DOX cardiac toxicity, and this was tested using 200 μM of rosmarinic acid. This effect did not affect the activity of DOX–PEG on MDA-231 breast cancer cells, where the IC_{50} of DOX–RosA–PEG at 200 μM of RosA was 2.4 μM, which is slightly higher than the IC_{50} observed when using DOX–PEG alone (2 μM). On the other hand, cardiac H9c2 cells were the most affected by treatment with DOX–PEG, measuring 0.8 μM IC_{50}, which is the lowest among the tested cells. Interestingly, coating DOX with RosA and PEG markedly reduced the toxic effect of DOX–PEG, scoring an IC_{50} of 4.4 μM when coating DOX–PEG with 200 μM of RosA.

Gene expression profile after doxorubicin treatment

Consistent with the extent of toxicity to doxorubicin, changes in expression were determined for RNA extracted from cells after doxorubicin treatment. A substantial fold change was considered with a cut-off point of 1.5. Initial results showed that 10 genes were up-regulated, and 48 genes were down-regulated. Further classification by DAVID (Table 2) annotation tool elucidated that most upregulated genes are involved in cardiac remodeling, cell growth, sarcomere structural proteins, and stress and immune response stress, while down regulated genes function in apoptosis, drug metabolism, transcriptional regulation, cell cycle, and signal transduction, or act as a transporter.

Gene expression profile after Dox–RosA–PEG–CS NP treatment

The genetic profile of cells exposed to Dox–RosA–PEG–CS NPs revealed that only one gene was upregulated and involved in the cell growth pathway (Table 3). On the other hand, 53 genes were downregulated and found to be involved in apoptosis, cardiac remodeling, cell cycle regulation, stress response, and transcriptional regulation (Table 3).

Discussion

The rosmarinic acid–doxorubicin–PEG–chitosan (Dox–RosA–PEG–CS) system is a notable example, showcasing promising characteristics for targeted cancer treatment. The reported particle size of Dox–RosA–PEG–CS, approximately 305 ± 5 nm, ensures optimal circulation and tumor penetration. At the same time, the zeta potential of +14.2 mV suggests enhanced cellular uptake due to electrostatic interactions with negatively charged cell membranes. Furthermore, the high encapsulation efficiency of DOX in this system (82%) highlights its capability to load and deliver the chemotherapeutic drug effectively. Infrared spectral data provide evidence of successful functionalization and interactions within the nanoparticle system, with peaks at 3440 cm^{-1} indicative of hydroxyl group stretching, 2360 cm^{-1} signaling potential carbon dioxide adsorption, and 542 cm^{-1} attributed to metal–oxygen or polymer complex vibrations. Together, these features position Dox–RosA–PEG–CS nanoparticles as a robust platform for enhanced drug delivery, offering improved stability, controlled drug release, and potential for reduced systemic toxicity in cancer treatment.

With IC_{50} values of 2 and 0.8 μM on MDA-231 and H9c2 cardiac cells, respectively, DOX–PEG demonstrated substantial toxicity to the examined cells. The chemotherapy medication doxorubicin exhibited exceptional toxicity to heart cells. In line with our theory, it was proposed that DOX cardiac toxicity could be reduced by combining doxorubicin and RosA in a single medication (DOX–RosA–PEG). Our findings demonstrated that RosA can, in a dose-dependent manner, shield cardiac cells from the negative effects of DOX. The activity of DOX-PEG on

MDA-231 breast cancer cells was unaffected by this impact; the IC_{50} of DOX–RosA–PEG at 200 of RosA was 2.4 μM, marginally higher than the IC_{50} of DOX–PEG alone (2 μM). Consistent with the above, cardiac H9C2 cells were the most affected by treatment with DOX–PEG, measuring 0.8 μM IC_{50}, the lowest among the tested cells. Interestingly, coating DOX with RosA and PEG markedly reduced the toxic effect of DOX–PEG, scoring an IC_{50} of 4.4 μM when coating DOX–PEG with 200 μM of RosA. Altogether, our data show the toxic effect of DOX–PEG on cancer and normal cell types, with modest toxicity observed on cardiac cells. RosA showed a protective effect on normal cells, and a modest protective effect was observed on H9c2 cardiac cells. In contrast, RosA slightly reduced the toxic effect of DOX–PEG against MDA-231 breast cancer cells, but this effect is considered negligible.

DOX is a useful anticancer medication with a wide therapeutic range. However, its adverse effects, which include cardiotoxicity, cardiac remodeling, and chronic heart failure, significantly restrict its clinical use.[20] Numerous studies have been conducted on congestive heart failure and DOX-induced cardiotoxicity. Nevertheless, the molecular processes behind these negative effects remain unclear. Furthermore, there aren't many clinically available medications that effectively prevent DOX-induced cardiotoxicity. The extract known as RosA is made up of numerous botanicals. It has been linked to a number of health advantages. While it has a variety of biological functions in humans, such as antiviral, antibacterial, antioxidant, antimutagenic, and anti-inflammatory qualities, it acts as a defensive chemical in plants. Its capacity to suppress pro-inflammatory cytokines, including interleukin (IL)-1β, tumor necrosis factor-alpha (TNF-α), and IL-6, is what gives it its anti-inflammatory qualities.[21] However, whether and how RosA enhances cardiac function and reduces myocardial remodeling in DOX-induced cardiotoxicity is unclear. In this research, we investigated the protective effects of RosA on H9c2 cells subjected to DOX-induced cardiotoxicity. Our findings indicated that while DOX treatment led to cardiotoxicity, RosA provided cardio-protection against this effect in H9c2 cells. We observed that RosA reduced apoptosis and inflammation, enhanced angiogenesis, and diminished myocardial fibrosis by decreasing collagen production. These findings illustrated that RosA mitigates DOX-induced apoptosis, myocardial fibrosis, cardiac remodeling, and inflammatory responses in H9c2 cells.

In the current study, DOX successfully caused toxicity in the cells. The cardiovascular disease PCR array results indicated that the levels of cell cycle, transcriptional regulation, and signal transduction were significantly reduced. At the same time, cardiac remodeling, sarcomere structural proteins, and inflammatory response were significantly elevated in the Dox-treated cells compared to the control cells. Nevertheless, RosA was able to reverse most of these transcriptomic alterations. These findings suggest that RosA may have the potential to enhance myocardial function in cardiac cells affected by DOX.

Angiogenesis plays a crucial role in the repair process following myocardial ischemia. The stimulation of angiogenesis is expected to reduce ventricular dysfunction and remodeling in cells affected by DOX.[22] Additionally, alterations in the transcription levels of apoptosis factors such as Maoa and Ndufb5 influence the sensitivity to mitochondrial apoptosis. Changes in the transcript levels of natriuretic peptide precursorsA and B, which serve as early and sensitive markers of doxorubicin-induced cardiotoxicity, might be associated with apoptosis in myocardial infarction.[23] Our findings indicated that RosA offers protection to cardiac cells against DOX-induced toxicity by downregulating natriuretic peptide precursor A and B, compared to cells treated only with doxorubicin.

Previous research has indicated that Wnt signaling plays a role in the cardiotoxic effects caused by doxorubicin.[24,25] The Wnt/β-catenin signaling pathway inhibits apoptosis and provides a protective mechanism against cardiotoxicity induced by doxorubicin, suppressing this signaling pathway.[26] This pathway is essential for various developmental processes, including heart formation and homeostatic functions such as apoptosis, cell growth, migration, and differentiation.[27] A group of proteins related to Wnt signaling, particularly the secreted frizzled-related protein 4 (sFRP4), exhibits location-dependent responses to the cardiotoxic effects of DOX.[28] Treatment with doxorubicin leads to an increase in the extracellular release of sFRP4.[29] Blocking the secretion of sFRP has been shown to reduce doxorubicin-induced cardiotoxicity *in vitro* by activating the Wnt/β-catenin signaling pathway. The level of Sfrp4 was significantly increased in the doxorubicin-treated cells compared to the control group. However, RosA was able to suppress the overexpression of Sfrp4. Therefore, RosA may reduce cardiac inflammation and apoptosis induced by DOX in H9c2 cells.

Chemokines are a group of small cytokines with chemotactic properties that control the movement of immune cells toward target tissues. Chemokines play a crucial role in directing leukocytes to areas of inflammation. Additionally, chemokines may influence cardiovascular diseases by affecting leukocyte activation, monocyte survival, foam cell development, thrombus formation, and lymphangiogenesis. Complement component 6 (CCL11) has been shown to play a vital role in cardiovascular diseases and heart failure.[30] CCL11 serves as the primary chemoattractant for neutrophils, while also attracting monocytes. Besides its function in chemotaxis, CCL11 can promote cardiac fibrosis through TGF SMAD 2/3 signaling.[31] In H9C2 cells, CCL11 is significantly increased following DOX NP treatment compared to the control group. Nonetheless, RosA suppressed the overexpression of CCL11. Therefore, RosA could reduce cardiac inflammation caused by DOX in H9c2 cells.

Alongside CCL11, C–C motif chemokine ligand 2 (CCL2) is crucial for attracting classical monocytes (pro-inflammatory $CD14^{+}CD16^{-}$ monocytes) and contributing to the onset of cardiotoxicity. CCL2 is released by immune cells, smooth muscle cells, endothelial cells, and fibroblasts. The CCL2/CCR2 pathway governs the movement of various immune cells such as monocytes, macrophages, T cells, and NK cells. Plasma concentrations of CCL2 have been linked to a heightened risk for heart failure, atherosclerosis, and coronary artery disease.[31] In a preclinical model, CCL2/CCR2 was found to be essential for atherosclerosis development, with the selective removal of CCR2 resulting in a notable reduction in atherosclerotic lesions

and a decrease in monocyte/macrophage accumulation. Moreover, the lack of CCR2 diminished the infiltration of Ly6C^{high} monocytes into the infarction area and suppressed inflammation. A decrease in inflammatory monocytes facilitated the healing of myocardial infarctions.[32] In the current investigation, we observed that CCL2 was significantly increased in the Dox-treated H9c2 cells compared to the control cells but decreased following RosA treatment.

Cardiac troponin, particularly troponin I (Tnni3) and T (Tnnt2), is present in cardiac myocytes and is released into the bloodstream when there is a breach in sarcolemmal integrity. In clinical settings, troponin is a sensitive and specific indicator of myocardial damage, commonly assessed during acute myocardial infarction for both diagnostic and prognostic purposes.[33] Nonetheless, troponin levels may be increased in various conditions, including hypertensive crises, kidney failure, rhabdomyolysis, sepsis, chronic poor vascular conditions, and drug-related cardiotoxicity.[34] The usefulness of troponin in cardiotoxicity caused by DOX has been shown in animal studies. Herman and his team demonstrated a positive relationship between increasing Tnni3 levels and cumulative doses of doxorubicin in spontaneously hypertensive rats.[34] Our research yielded similar results, indicating that the Tnni3 and Tnnt2 transcripts were significantly upregulated and contributed to cardiotoxicity in DOX-treated H9C2 cells. Nonetheless, the inclusion of RosA diminished the stress induced by DOX. When H9C2 cells received treatment with both RosA and DOX, the toxicity induced by DOX was notably alleviated, thereby validating the protective effects of RosA.

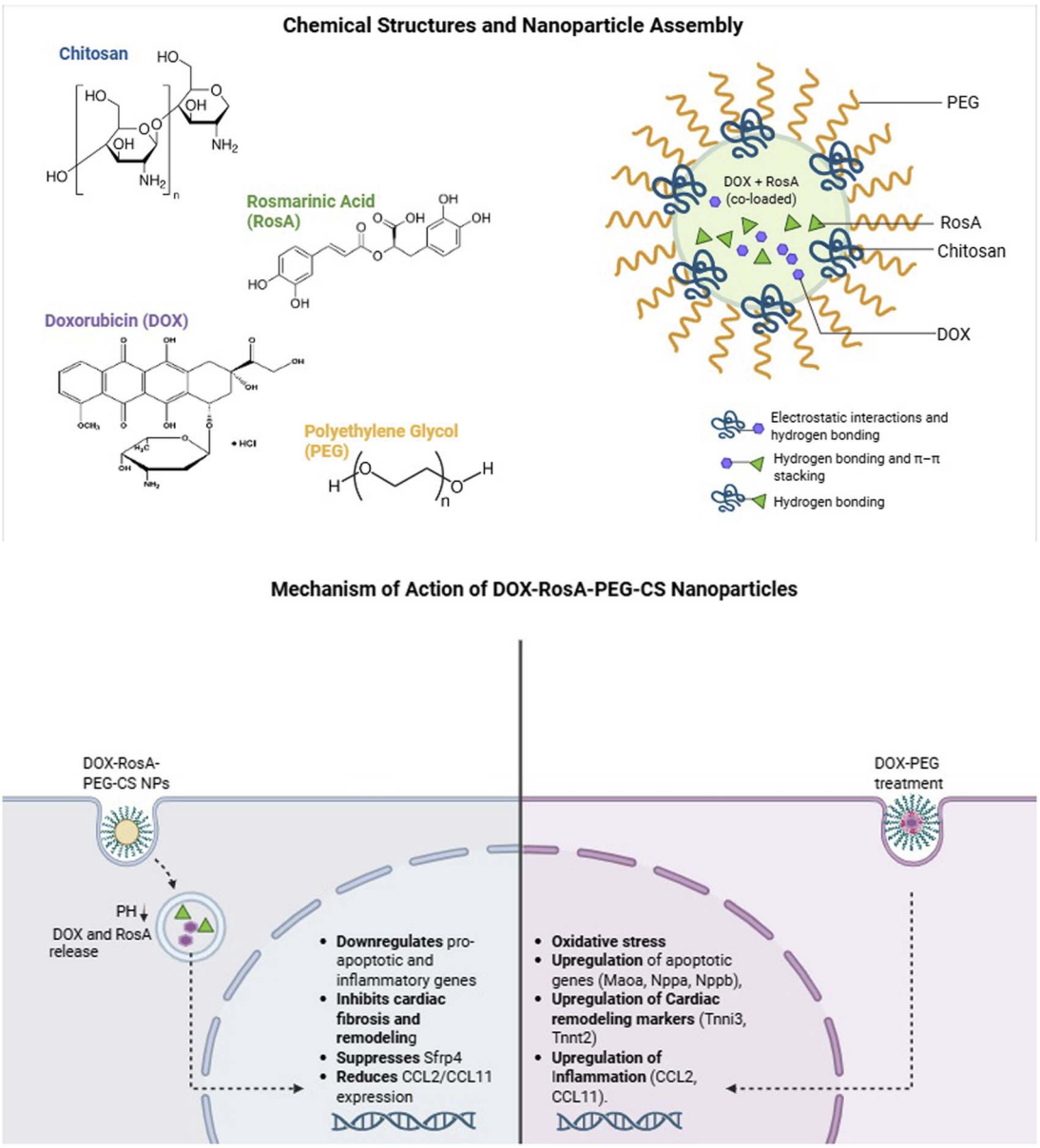

Fig. 3 (a) Illustrating the chemical structure of each nanoparticle component (doxorubicin, rosmarinic acid, PEG, and chitosan), (b) a schematic representation of the possible mechanism of action for the synthesized nanoparticles.

As shown in Fig. 3a, doxorubicin was encapsulated and stabilized within the nanoparticle matrix *via* electrostatic interactions and hydrogen bonding with PEGylated chitosan. Rosmarinic acid (RosA) was conjugated through hydrogen bonding and π–π stacking interactions with DOX, thereby enhancing its bioactivity and protective action. Moreover, PEG served as a stealth layer, enhancing systemic circulation and biocompatibility through hydrophilic surface modification, while chitosan provided a cationic backbone enabling cell membrane interaction and pH-responsive drug release. Regarding the possible mechanism of action of the synthesized NPs, the Dox–RosA–PEG–CS NPs preferentially accumulate in tumor tissues due to the enhanced permeability and retention effect. Once internalized by cancer cells (MDA-MB-231), acidic endosomal pH triggers the release of DOX, which intercalates into DNA and inhibits topoisomerase II, leading to apoptosis. RosA, a polyphenol with anti-inflammatory and antioxidant properties, enhances the efficacy of DOX while mitigating oxidative stress and inflammation in surrounding healthy tissues, particularly in cardiomyocytes (H9c2 cells). Importantly, RosA exerts anti-inflammatory and anti-fibrotic effects by downregulating pro-inflammatory cytokines (*e.g.*, CCL2, CCL11) and natriuretic peptides (Nppa/Nppb), as demonstrated in our transcriptomic analysis (Fig. 3b).

Conclusion

In the current study, doxorubicin–rosmarinic acid–PEG–chitosan (DOX–RA–PEG–CS) nanoparticles represent a novel therapeutic system with significant advantages in cancer treatment. These nanoparticles, with a hydrodynamic size of 305 ± 5 nm, a zeta potential of +14.2 mV, and an encapsulation efficiency of 82%, offer improved delivery and efficacy of doxorubicin while mitigating its associated cardiotoxicity. The system demonstrated a significant cardioprotective effect against DOX-induced toxicity in H9c2 cells. RosA prevented apoptosis, inflammation, and fibrosis in cardiomyocytes. Our results suggest that RosA provides its protective benefits by blocking multiple signaling pathways that lead to apoptosis and inflammation. Furthermore, to the best of our knowledge, this is the first study to document the myocardial protective effect of RosA. Nevertheless, this finding necessitates further empirical confirmation. The NP delivery system further enhanced the therapeutic benefits of the RosA–DOX combination, offering a novel approach for reducing systemic toxicity and improving targeted action. These findings provide critical insights into the cardioprotective mechanisms of RosA and its potential application as an adjunctive therapy in oncology. RosA could potentially address DOX-induced cardiotoxicity by influencing targeted cardiac remodeling genes.

Conflicts of interest

The authors declare no conflict of interest, financial or otherwise.

Data availability

The authors confirm that the data supporting the findings of this research are available within the article.

Acknowledgements

The authors would like to thank the Science Research Fund, the Ministry of Higher Education, and Scientific Research-Jordan for the financial support of this project (Grant number MPH/1/61/2021).

References

1 Y. Y. Zhang, M. Yi and Y. P. Huang, Oxymatrine ameliorates doxorubicin-induced cardiotoxicity in rats, *Cell. Physiol. Biochem.*, 2017, **43**(2), 626–635.
2 S. Chakraborti, A. Pramanick, S. Saha, *et al.*, Atypical G protein β5 promotes cardiac oxidative stress, apoptosis, and fibrotic remodeling in response to multiple cancer chemotherapeutics, *Cancer Res.*, 2018, **78**(2), 528–541.
3 C. F. Thorn, C. Oshiro, S. Marsh, T. Hernandez-Boussard, H. McLeod, T. E. Klein, *et al.*, Doxorubicin pathways: pharmacodynamics and adverse effects, *Pharmacogenet. Genomics*, 2011, **21**(7), 440–446.
4 L. Sodagam, A. Lewinska, E. Kwasniewicz, S. Kokhanovska, M. Wnuk and K. Siems, Phytochemicals rosmarinic acid, ampelopsin, and amorfrutin-A can modulate age-related phenotype of serially passaged human skin fibroblasts *in vitro*, *Front. Genet.*, 2019, **10**, 81.
5 J. Govender, B. Loos, E. Marais and A. M. Engelbrecht, Mitochondrial catastrophe during doxorubicin-induced cardiotoxicity: a review of the protective role of melatonin, *J. Pineal Res.*, 2014, **57**, 367–380.
6 Y. Shi, M. Moon, S. Dawood, B. McManus and P. P. Liu, Mechanisms and management of doxorubicin cardiotoxicity, *Herz*, 2011, **36**, 296–305, DOI: **10.1007/s00059-011-3470-3**.
7 M. Petersen and M. S. J. Simmonds, Rosmarinic acid, *Phytochemistry*, 2003, **62**(2), 121–125.
8 G. Bozzuto, A. Calcabrini, M. Colone, M. Condello, M. L. Dupuis and E. Pellegrini, *et al.*, Phytocompounds and nanoformulations for anticancer therapy: a review, *Molecules*, internet, 2024, **29**, 16, 3784, cited 2025 Apr 9, available from: **https://www.mdpi.com/1420-3049/29/16/3784**.
9 A. Das, S. Adhikari, D. Deka, N. Baildya, P. Sahare and A. Banerjee, *et al.*, An updated review on the role of nanoformulated phytochemicals in colorectal cancer, *Medicina*, internet, 2023, **59**, 4, 685, cited 2025 Jul 5, available from: **https://www.mdpi.com/1648-9144/59/4/685**.
10 A. Sharmila and S. C. Immanuel, Facile synthesis of xanthan gum-based sheets loaded with ganoderic acid F for evaluation of therapeutic potential, molecular docking, and ADMET profiling, *Int. J. Biol. Macromol.*, 2025, **322**(1), 146619.

11 A. Al-Hunaiti, A. Gazzy, H. Aqel, T. Abu Thiab, R. Saeed, M. Taha, *et al.*, New chitosan-based trimetallic $Cu_{0.5}Zn_{0.5}Fe_2O_4$ nanoparticles: preparation, characterization, and anti-cancer activity, *Pharm. Pract.*, 2024, **22**(4), 1.

12 A. Al-Hunaiti, M. Zihlif, T. Abu Thiab, W. Al-Awaida, H. J. Al-Ameer and A. Imraish, Magnetic nanoparticle-based combination therapy: synthesis and *in vitro* proof of concept of $CrFe_2O_4$-rosmarinic acid nanoparticles for anti-inflammatory and antioxidant therapy, *PLoS One*, 2024, **19**(8), e0297716.

13 M. Florescu, M. Cinteză and D. Vinereanu, Chemotherapy-induced cardiotoxicity, *Maedica*, 2013, **8**(1), 59–67.

14 R. Harishkumar and C. I. Selvaraj, Lotusine, an alkaloid from Nelumbo nucifera (Gaertn.), attenuates doxorubicin-induced toxicity in embryonically derived H9c2 cells, *In Vitro Cell. Dev. Biol.: Anim.*, 2020, **56**, 367–377.

15 R. HarishKumar and C. I. Selvaraj, Nuciferine from Nelumbo nucifera Gaertn. attenuates isoproterenol-induced myocardial infarction in Wistar rats, *Biotechnol. Appl. Biochem.*, 2022, **69**(3), 1176–1189.

16 R. Harishkumar, M. S. Manjari, C. Rose, *et al.*, Protective effect of *Nelumbo nucifera* (Gaertn.) against H_2O_2-induced oxidative stress on H9c2 cardiomyocytes, *Mol. Biol. Rep.*, 2020, **47**, 1117–1128.

17 V. M. Hadkar, C. Mohanty and C. I. Selvaraj, Biopolymeric nanocarriers in cancer therapy: unleashing the potency of bioactive anticancer compounds for enhancing drug delivery, *RSC Adv.*, 2024, **14**, 25149–25173.

18 W. Tan, Q. Li, F. Dong, J. Zhang, F. Luan, L. Wei, *et al.*, Novel cationic chitosan derivative bearing 1,2,3-triazolium and pyridinium: synthesis, characterization, and antifungal property, *Carbohydr. Polym.*, 2018, **182**, 180–187.

19 S. Xie, C. Chang, R. Jiang, *et al.*, Network pharmacology and experimental verification: rosmarinic acid alleviates doxorubicin-induced cardiomyocyte apoptosis by regulating BCL2L1, *Hum. Exp. Toxicol.*, 2025, **44**, DOI: **10.1177/09603271251354890**.

20 R. Vikram, K. Jaspal and M. Nilotpal, Emerging trends in cancer nanomedicine: the road to precision oncology, *Adv. Drug Delivery Rev.*, 2021, **178**, 113967.

21 S. Wilhelm, A. J. Tavares, Q. Dai, *et al.*, Analysis of nanoparticle delivery to tumours, *Nat. Rev. Mater.*, 2016, **1**(5), 16014.

22 A. Imraish, T. Abu Thiab, W. Al-Awaida, H. J. Al-Ameer, Y. Bustanji and H. Hammad, *In vitro* anti-inflammatory and antioxidant activities of $ZnFe_2O_4$ and $CrFe_2O_4$ nanoparticles synthesized using *Boswellia carteri* resin, *J. Food Biochem.*, 2021, **45**, e13730.

23 M. Bauch, A. Ester, B. Kimura, B. E. Victorica, A. Kedar and M. I. Phillips, Atrial natriuretic peptide as a marker for doxorubicin-induced cardiotoxic effects, *Cancer Res.*, 1992, **52**(6), 1492–1496.

24 Y. Hu, Z. Wang, Y. Xu, Y. Zhang, X. Jiang and Z. Lin, sFRP1 protects H9c2 cardiac myoblasts from doxorubicin-induced apoptosis by inhibiting the Wnt/PCP-JNK pathway, *Acta Pharmacol. Sin.*, 2020, **41**(7), 1150–1157.

25 L. Liang, M. Zhang, X. Guo, H. Wang, L. Wang, D. Meng, *et al.*, Dkk1 exacerbates doxorubicin-induced cardiotoxicity by inhibiting the Wnt/β-catenin signaling pathway, *J. Cell Sci.*, 2019, **132**(14), jcs228478.

26 K. H. Chen, Y. S. Chen, Z. H. Wang, J. Xu, X. Xie, W. Liang, *et al.*, Combined therapy with melatonin and exendin-4 effectively attenuated the deterioration of renal function in rat cardiorenal syndrome, *Am. J. Transl. Res.*, 2017, **9**(1), 214–229.

27 R. Nusse and H. Clevers, Wnt/β-catenin signaling, disease, and emerging therapeutic modalities, *Cell*, 2017, **169**(6), 985–999.

28 C. L. Wu, R. Yin, S. N. Wang and R. Ying, A review of CXCL1 in cardiac fibrosis, *Front. Cardiovasc. Med.*, 2021, **8**, 674498.

29 Y. L. Zhang, H. J. Cao, X. Han, F. Teng, C. Chen, J. Yang, *et al.*, Chemokine receptor CXCR-2 initiates atrial fibrillation by triggering monocyte mobilization in mice, *Hypertension*, 2020, **76**(2), 381–392.

30 C. Rosales, Neutrophil: a cell with many roles in inflammation or several cell types?, *Front. Physiol.*, 2018, **9**, 113.

31 L. R. Yu, Z. Cao, I. Makhoul, J. R. Daniels, S. Klimberg, J. Y. Wei, *et al.*, Immune response proteins as predictive biomarkers of doxorubicin-induced cardiotoxicity in breast cancer patients, *Exp. Biol. Med.*, 2017, **242**(15), 1386–1395.

32 M. Roffi, C. Patrono, J. P. Collet, C. Mueller, M. Valgimigli, F. Andreotti, *et al.*, 2015 ESC guidelines for the management of acute coronary syndromes in patients presenting without persistent ST-segment elevation, *Eur. Heart J.*, 2016, **37**(3), 267–315.

33 K. B. Wallace, E. Hausner, E. Herman, G. D. Holt, J. T. MacGregor, A. L. Metz, *et al.*, Serum troponins as biomarkers of drug-induced cardiac toxicity, *Toxicol. Pathol.*, 2004, **32**(1), 106–121, DOI: **10.1080/01926230490253696**.

34 E. Herman, S. E. Lipshultz, N. Rifai, J. Zhang, T. Papoian, Z. Yu, *et al.*, Use of cardiac troponin T levels as an indicator of doxorubicin-induced cardiotoxicity, *Cancer Res.*, 1998, **58**, 195–217.